Bayesian modal identification method based on general coherence model for asynchronous ambient data

Yi-Chen Zhu[1] and Siu-Kui Au[2]

Abstract

A Bayesian frequency domain method for modal identification using asynchronous ambient data has been proposed previously. It provides a flexible and economical way to conduct ambient vibration tests as time synchronisation among data channels is not required. To simplify computation, zero coherence among synchronous data groups is assumed in the method, which inevitably introduces modelling error and lacks the ability of quantifying the synchronisation degree among different groups. To address these issues, a Bayesian modal identification method with a general coherence assumption among synchronisation groups is proposed in this paper. Computational difficulties are addressed and an efficient algorithm for determining the most probable values of modal properties is proposed. Synthetic and laboratory data examples are presented to validate the proposed method. It is also applied to modal identification of a full-scale ambient test, which illustrates the feasibility of the proposed method to real asynchronous data under field test configurations. For the cases investigated the proposed method does not lead to significant improvement in the identification accuracy of modal parameters compared to the method with zero coherence assumption. This is consistent with previous experience regarding the robustness of the zero coherence assumption and is now verified in this work. One may use the latter in practice for computational efficiency if the synchronisation degree among different groups is not demanded.

Key Words: Ambient data; Asynchronous data; Bayesian methods; General coherence model; Operational modal analysis

[1] Corresponding author. Email: yichen.zhu@sheffield.ac.uk. Dynamic Research Group, Department of Mechanical Engineering, The University of Sheffield, UK.
[2] Email: ivanau@ntu.edu.sg. School of Civil & Environmental Engineering, Nanyang Technological University, Singapore. Formerly with Institute for Risk and Uncertainty and Centre for Engineering Dynamics, University of Liverpool, UK.

1. Introduction

Operational Modal Analysis (OMA) has been widely used in structural health monitoring (SHM) to estimate the dynamic characteristics of real structures (e.g., natural frequencies, damping ratios and mode shapes) based on ambient vibration tests [1,2]. This is essential information that can be further applied in SHM including assessing the physical condition of structures or even detecting damage in structures during their service life [3–6]. Compared with other vibration tests like forced and free vibration tests, ambient vibration tests do not require artificial excitation but make full use of natural excitations such as wind, microtremor and traffic. Due to its high economy and efficiency in implementation, OMA has attracted great attention with a significant number of field tests performed [7–9].

Various kinds of OMA methods have been developed in both non-Bayesian and Bayesian contexts over the past decades. Peak-picking [10] and frequency-domain decomposition [11] are popular non-Bayesian approaches that provide a quick estimation of the modal properties. Stochastic subspace identification (SSI) method [12–14] has been widely used where the modal parameters are estimated by standard linear regression through a state-space model. On the other hand, Bayesian methods view OMA as a probabilistic inference problem. Determining the most probable modal properties involves maximising the posterior probability function of modal parameters for given measured data and modelling assumptions. A number of approaches have been developed, including time domain method [15], frequency domain method based on sample power spectral density [16–18] and fast Fourier transform (FFT) of data [19,20]. Recent applications include [21,22] using FFT of data and [23,24] based on sample power spectral density. It should be noted that, among the different formulations, the one based on FFT is preferred for its robustness to modelling assumptions (as compared to time domain method) and fundamental nature (not involving averaging concept as in spectral density method) [2].

Conventional OMA methods require ‘synchronous’ data, where different data channels should start sampling at the same time and at the same pace thereafter. In real implementation, time synchronisation is a crucial issue that should be considered and planned. In one conventional configuration, the analogue data from different sensors are transmitted to a central data acquisition (DAQ) unit that controls the sampling process. This requires long cables in full-scale tests, which leads to additional noise in the measured data and logistics costs. Other time synchronisation schemes include Network Time Protocol [25], Global

Positioning System (GPS) [26] and wireless sensor networks [27–29] that require additional instruments and overheads in field deployment. Field tests can be conducted in a more economical and efficient manner if OMA can be performed using asynchronous ambient data.

Asynchronisation is mainly caused by two factors, the initial time shift (start time) between channels and the random time drift due to different sampling clocks. The initial time shift can be detected and aligned using existing time delay estimation methods [30,31]. Compared to initial time shift, random time drift cannot be easily aligned and is the primary issue in real applications when multiple DAQ units are used without synchronisation. Asynchronisation due to random time drifts accumulates over time, which leads to the non-stationary behaviour in the sampled data. Recently, an asynchronous model has been proposed for OMA [32]. It assumes the data to be stationary within suitable time scales in order to facilitate analysis while capturing key asynchronous characteristics through imperfect coherence. Based on this model, a Bayesian OMA method has been developed assuming zero coherence among different synchronisation data groups [33,34]. It provides a quick estimation of modal parameters and associated identification uncertainties based on asynchronous ambient data. Inevitably, it involves extra modelling error (real asynchronous data may not have zero coherence among different groups) and lacks the ability of estimating the synchronisation degree among different groups.

To address these challenges, this paper proposes a Bayesian OMA method based on the asynchronous data model with general coherence assumption. It accounts for the asynchronous characteristics in the measured data when making inference about the modal parameters and is capable of determining the MPV of coherence values among different synchronous data groups. The identification procedure based on the asynchronous data model with general coherence values turns out to be computationally non-trivial and ill-conditioned. Efficient strategies for numerical optimisation are developed to suppress the dimension of matrix involved in computation. Consequently, Bayesian modal identification can be performed efficiently using the proposed method based on asynchronous ambient data. The proposed method is illustrated using both synthetic and laboratory data. It is also applied to modal identification of a full-scale structure which investigates the challenges encountered when using asynchronous data for OMA in a practical context.

2. Bayesian frequency domain method

The modal identification method proposed in this work is based on a Bayesian frequency domain approach using the Fast Fourier transform (FFT) of measured ambient data. The overall formulation is reviewed in this section. Let the measured ambient acceleration data be $\left\{\hat{\ddot{\mathbf{x}}}_j \in R^n\right\}_{j=1}^N$ with n degrees of freedom (DOF) of the subject structure and N sampling points per channel. The data are assumed to consist of structural response $\ddot{\mathbf{x}}_j \in R^n$ as well as prediction error $\boldsymbol{\varepsilon}_j \in R^n$ arising from modelling error and measurement noise:

$$\hat{\ddot{\mathbf{x}}}_j = \ddot{\mathbf{x}}_j + \boldsymbol{\varepsilon}_j \tag{1}$$

Define the scaled FFT of measured data $\left\{\hat{\ddot{\mathbf{x}}}_j\right\}$ as:

$$\mathcal{F}_k = \sqrt{\frac{2\Delta t}{N}} \sum_{j=1}^{N} \hat{\ddot{\mathbf{x}}}_j \exp\left[-2\pi \mathbf{i} \frac{(k-1)(j-1)}{N}\right] \tag{2}$$

corresponding to frequency $\mathrm{f}_k = (k-1)/N\Delta t \,(\mathrm{Hz})$ for $k = 1,...N_q$. Here, $\mathbf{i}^2 = -1$; Δt is the sampling interval and $N_q = \mathrm{int}(N/2)+1$ (int(.) denotes integer part) is the index corresponding to the Nyquist frequency. The power spectral density (PSD) matrix of the measured data at frequency f_k can be calculated as multiplying $\mathcal{F}_k$ by its conjugate transpose. The scaling factor $\sqrt{2\Delta t / N}$ is defined such that the PSD is one-sided with respect to frequency in Hz.

Let $\{\mathcal{F}_k\}$ denote the set of FFT data within a selected frequency band for modal identification with N_f points in the set. In the context of Bayesian inference, the measured data depends on the set of modal parameters $\boldsymbol{\theta}$ to be identified, which normally includes natural frequencies, damping ratios, mode shapes, PSD of modal force and prediction error, etc. Using Bayes theorem and assuming a uniform prior (justified for OMA as the likelihood function is fast-varying compared to the prior PDF when data size is sufficiently large), the posterior PDF of $\boldsymbol{\theta}$ given $\{\mathcal{F}_k\}$ is proportional to the likelihood function, i.e.,

$$p\left(\boldsymbol{\theta} \middle| \{\mathcal{F}_k\}\right) \propto p\left(\{\mathcal{F}_k\} \middle| \boldsymbol{\theta}\right) \tag{3}$$

For high sampling rate and long data duration, it can be shown that $\{\mathcal{F}_k\}$ are asymptotically independent at different frequencies and jointly 'complex Gaussian' [35]. The likelihood function is then given by:

$$p\left(\{\mathcal{F}_k\}|\boldsymbol{\theta}\right)=(\pi)^{-nN_f}\times\prod_k\left(\det\mathbf{E}_k\right)^{-1}\exp\left[-\sum_k\mathcal{F}_k^{*}\mathbf{E}_k^{-1}\mathcal{F}_k\right] \tag{4}$$

where '*' denotes complex conjugate transpose and $\mathbf{E}_k = E[\mathcal{F}_k\mathcal{F}_k^{*}|\boldsymbol{\theta}]$ is the theoretical PSD matrix. It is convenient to work with the 'negative log-likelihood function' (NLLF) $L(\boldsymbol{\theta})$ such that

$$p\left(\boldsymbol{\theta}|\{\mathcal{F}_k\}\right)\propto\exp\left[-L(\boldsymbol{\theta})\right] \tag{5}$$

where

$$L\left(\boldsymbol{\theta}\right)=\sum_k\ln\det\mathbf{E}_k+\sum_k\mathcal{F}_k^{*}\mathbf{E}_k^{-1}\mathcal{F}_k \tag{6}$$

For sufficiently long data, the posterior PDF has a unique maximum (i.e., globally identifiable). The MPV of $\boldsymbol{\theta}$ can then be obtained by maximising the posterior PDF, or equivalently minimising the NLLF in Eq. (6).

3. Asynchronous data model in OMA

The Bayesian FFT method for asynchronous data in this paper is developed based on the asynchronous data model proposed in [32], which is briefly reviewed in this section. Modelling asynchronous data is difficult as it is fundamentally a non-stationary process. To keep the identification problem tractable, it is modelled as a stationary process with imperfect coherence to facilitate modal identification, while capturing the key asynchronous characteristics within suitable time scales. Based on this model, the theoretical PSD matrix $\mathbf{E}_k$ for asynchronous data can be derived.

Assume that the test configuration on time synchronisation is given, which is typically the case in real applications. Define a 'synchronous data group' as a set of data channels where the data are sampled synchronously (i.e., using the same clock). Let n_g denote the total number of synchronous data groups in the whole measurement array. Consider a frequency band dominated by a single mode. Let $\boldsymbol{\varphi}$ denote the 'global mode shape' covering all measured DOFs and $\mathbf{u}_i\in R^{n_i}$ denote the part of $\boldsymbol{\varphi}$ measured by the ith synchronous data group with n_i DOFs, i.e.

$$\boldsymbol{\varphi} = \begin{bmatrix} \mathbf{u}_1 \\ \vdots \\ \mathbf{u}_{n_g} \end{bmatrix} \tag{7}$$

Let $\ddot{\eta}_{ki}$ be the FFT of the modal acceleration $\ddot{\eta}_i(t)$ associated with the ith synchronous data group. The FFT of the measured asynchronous data now can be modelled as:

$$\mathcal{F}_k = \begin{bmatrix} \mathbf{u}_1 \ddot{\eta}_{k1} \\ \vdots \\ \mathbf{u}_{n_g} \ddot{\eta}_{kn_g} \end{bmatrix} + \boldsymbol{\varepsilon}_k \tag{8}$$

The modal acceleration $\ddot{\eta}_i(t)$ satisfies the modal equation of motion (assuming classically damped structure):

$$\ddot{\eta}_i(t) + 2\zeta\omega\dot{\eta}_i(t) + \omega^2\eta_i(t) = p_i(t) \qquad i = 1,\ldots,n_g \tag{9}$$

where $\omega = 2\pi f$ (rad/s); f (Hz) and ζ are the natural frequency and damping ratio of the mode, respectively; $p_i(t)$ is the modal force associated with the ith synchronous data group.

For synchronous data, $p_i(t)$ among different groups are identical and so are $\ddot{\eta}_{ki}$. This is not the case for asynchronous data, however. Assuming the same measurement duration for all the data channels (i.e., start recording at the same time with the same number of sampling points) while different synchronous groups sample the data asynchronously. It is then reasonable to assume that the measured modal force among different groups are identically distributed, i.e.,

$$E\left(p_{ki}p_{ki}^*\right) = S \qquad i = 1,\ldots,n_g \tag{10}$$

such that

$$E\left(\ddot{\eta}_{ki}\ddot{\eta}_{ki}^*\right) = SD_k \qquad i = 1,\ldots,n_g \tag{11}$$

where S is the modal force PSD (assuming a constant PSD within the band) and

$$D_k = \left[\left(\beta_k^2 - 1\right)^2 + \left(2\zeta\beta_k\right)^2\right]^{-1} \qquad \beta_k = f/\mathrm{f}_k \tag{12}$$

is the dynamic amplification factor.

Balancing relevance and simplicity, the relationship of modal acceleration among different synchronous groups are (empirically) modelled through imperfect coherence:

$$\chi_{ij} = \frac{E\left(\ddot{\eta}_{ki}\ddot{\eta}_{kj}^{*}\right)}{\sqrt{E\left(\ddot{\eta}_{ki}\ddot{\eta}_{ki}^{*}\right)E\left(\ddot{\eta}_{kj}\ddot{\eta}_{kj}^{*}\right)}} \tag{13}$$

where $\chi_{ij} \in C$ ($\left|\chi_{ij}\right| \le 1$) is the coherence between the ith and jth group. It is assumed to be constant within the selected band, which is justified when the selected band is not wide (typical in real applications). Modelling the prediction error as i.i.d. (independent and identically distributed) with a constant PSD S_e for all the data channels in the selected band, the resulting PSD matrix for asynchronous data now can be written as:

$$\mathbf{E}_k = E\left(\mathcal{F}_k\mathcal{F}_k^{*}\right) = SD_k\begin{bmatrix} \mathbf{u}_1\mathbf{u}_1^T & \chi_{12}\mathbf{u}_1\mathbf{u}_2^T & \cdots & \chi_{1n_g}\mathbf{u}_1\mathbf{u}_{n_g}^T \\ \bar{\chi}_{12}\mathbf{u}_2\mathbf{u}_1^T & \mathbf{u}_2\mathbf{u}_2^T & & \vdots \\ \vdots & & \ddots & \vdots \\ \bar{\chi}_{1n_g}\mathbf{u}_{n_g}\mathbf{u}_1^T & \cdots & \cdots & \mathbf{u}_{n_g}\mathbf{u}_{n_g}^T \end{bmatrix} + S_e\mathbf{I}_n \tag{14}$$

As shown in Eq.(6), minimising the NLLF for determining the MPV of modal parameters requires repeated evaluations of the determinant and inverse of the PSD matrix $\mathbf{E}_k$ for different values of k and different trails of $\boldsymbol{\theta}$. It is of interest to know the characteristics of the determinant and inverse of $\mathbf{E}_k$. First rewrite $\mathbf{E}_k$ in Eq. (14) as

$$\mathbf{E}_k = SD_k\mathbf{U}\mathbf{C}\mathbf{U}^T + S_e\mathbf{I}_n \tag{15}$$

where

$$\mathbf{U} = \begin{bmatrix} \bar{\mathbf{u}}_1 & & \\ & \ddots & \\ & & \bar{\mathbf{u}}_{n_g} \end{bmatrix} \tag{16}$$

$$\mathbf{C} = diag\left\{\left\|\mathbf{u}_i\right\|\right\}_{i=1}^{n_g}\boldsymbol{\chi}\,diag\left\{\left\|\mathbf{u}_i\right\|\right\}_{i=1}^{n_g} \tag{17}$$

Here, $\bar{\mathbf{u}}_i = \mathbf{u}_i / \left\|\mathbf{u}_i\right\|$, $diag\left\{\left\|\mathbf{u}_i\right\|\right\}_{i=1}^{n_g}$ denotes a diagonal matrix with entries $\left\{\left\|\mathbf{u}_i\right\|\right\}_{i=1}^{n_g}$ and $\boldsymbol{\chi}$ denotes a $n_g \times n_g$ matrix with (i,j)-entry χ_{ij}. Let $\left\{\lambda_i \ge 0\right\}_{i=1}^{n_g}$ and $\left\{\mathbf{c}_i \in C^{n_g}\right\}_{i=1}^{n_g}$ denote the eigenvalues and eigenvectors (with unit norm) of $\mathbf{C}$, respectively. The eigenvector representation of $\mathbf{C}$ is then given by

$$\mathbf{C} = \sum_{i=1}^{n_g}\lambda_i\mathbf{c}_i\mathbf{c}_i^{*} \tag{18}$$

Substituting Eq.(18) into Eq.(15) gives:

$$\mathbf{E}_k = \sum_{i=1}^{n_g} SD_k \lambda_i \boldsymbol{\alpha}_i \boldsymbol{\alpha}_i^* + S_e \mathbf{I}_n \tag{19}$$

where

$$\boldsymbol{\alpha}_i = \mathbf{U}\mathbf{c}_i \qquad i = 1,..., n_g \tag{20}$$

Using the orthonormal properties of $\{\mathbf{c}_i\}_{i=1}^{n_g}$ (i.e, $\mathbf{c}_i^*\mathbf{c}_i = 1$ and $\mathbf{c}_i^*\mathbf{c}_j = 0$ for $i \neq j$) and $\mathbf{U}^T\mathbf{U} = \mathbf{I}_{n_g}$, an orthonormal basis $\{\mathbf{a}_i \in C^n\}_{i=1}^{n}$ can be formed with $\mathbf{a}_i = \boldsymbol{\alpha}_i$ ($i = 1,..., n_g$). Substituting $\mathbf{I}_n = \sum_{i=1}^{n} \mathbf{a}_i \mathbf{a}_i^*$ into Eq.(19) gives the eigenvector representation of $\mathbf{E}_k$:

$$\mathbf{E}_k = \sum_{i=1}^{n_g} \left(SD_k \lambda_i + S_e \right) \mathbf{a}_i \mathbf{a}_i^* + \sum_{i=n_g+1}^{n} S_e \mathbf{a}_i \mathbf{a}_i^* \tag{21}$$

The determinant of $\mathbf{E}_k$ then can be obtained as the product of the eigenvalues, i.e.,

$$\det \mathbf{E}_k = S_e^{n-n_g} \prod_{i=1}^{n_g} \left(SD_k \lambda_i + S_e \right) \tag{22}$$

The inverse of $\mathbf{E}_k$ has the same eigenvectors but reciprocal of eigenvalues:

$$\mathbf{E}_k^{-1} = \sum_{i=1}^{n_g} \left(SD_k \lambda_i + S_e \right)^{-1} \mathbf{a}_i \mathbf{a}_k^* + \sum_{i=n_g+1}^{n} S_e^{-1} \mathbf{a}_i \mathbf{a}_i^* \tag{23}$$

4. Identification strategies for general coherence assumption

As shown in Eq.(21), the eigenvalue λ_i and eigenvector $\mathbf{c}_i$ of $\mathbf{C}$ depend on the norm of the partial mode shapes $\|\mathbf{u}_i\|$ associated with different synchronous groups as well as the coherence $\boldsymbol{\chi}$ in a non-trivial manner. It is difficult to express directly the determinant and inverse of $\mathbf{E}_k$ in analytically tractable forms. The computation of the determinant and inverse of $\mathbf{E}_k$ is also ill-conditioned. In the resonant frequency band of the mode, $\mathbf{E}_k$ is dominated by the modal response (first term in Eq.(15)) and the prediction error (second term in Eq.(15)) is relatively small. In this context, $\mathbf{E}_k$ is close to being singular with a rank of at most n_g . Without resorting to brute-force numerical optimisation, the efficient computation of these quantities becomes the natural target. In this section, the identification procedure for general coherence are discussed and solution strategies are proposed.

A condensed full-ranked matrix is first proposed to facilitate computation. Define $\mathbf{E}'_k \in C^{n_g}$ as

$$\mathbf{E}'_k = SD_k\mathbf{C} + S_e\mathbf{I}_{n_g} \tag{24}$$

Similar to the case of $\mathbf{E}_k$, the determinant and inverse of $\mathbf{E}'_k$ then can be given by

$$\det \mathbf{E}'_k = \prod_{i=1}^{n_g} \left(SD_k\lambda_i + S_e \right) \tag{25}$$

$$\mathbf{E}'^{-1}_k = \sum_{i=1}^{n_g} \left(SD_k\lambda_i + S_e \right)^{-1} \mathbf{c}_i\mathbf{c}_i^* \tag{26}$$

This allows the determinant and inverse of $\mathbf{E}_k$ to be expressed in terms of $\mathbf{E}'_k$ as

$$\det\mathbf{E}_k = S_e^{n-n_g} \det\mathbf{E}'_k \tag{27}$$

$$\mathbf{E}_k^{-1} = \mathbf{U}\mathbf{E}'^{-1}_k\mathbf{U}^T + S_e^{-1}\left(\mathbf{I}_n - \mathbf{U}\mathbf{I}_{n_g}\mathbf{U}^T\right) \tag{28}$$

The resulting NLLF then can be written as:

$$L(\boldsymbol{\theta}) = \left(n - n_g\right) N_f \ln S_e + \sum_k \ln\det \mathbf{E}'_k + S_e^{-1}\left(d - d'\right) + \sum_k \mathcal{F}_k'^* \mathbf{E}'^{-1}_k \mathcal{F}'_k \tag{29}$$

where

$$d = \mathcal{F}_k \mathcal{F}_k^* \tag{30}$$

$$d' = \mathcal{F}_k'^* \mathcal{F}'_k \tag{31}$$

$$\mathcal{F}'_k = \mathbf{U}^T \mathcal{F}_k \tag{32}$$

Compared with the initial NLLF in Eq.(6), the dimension of the matrix involved in the resulting NLLF (Eq.(29)) has now been suppressed to n_g (the number of synchronous data groups), which is much smaller than n (the number of measured DOFs) in applications. The matrix $\mathbf{E}'_k$ in the NLLF has full rank so its determinant and inverse are well-defined. Based on this NLLF, an iterative scheme will be proposed in the following sections where the modal parameters are optimised in groups, leveraging on the fact that changing some of the parameters does not significantly affect the optimal value of others. In this context, the dimension of the optimisation problem is further reduced.

5. Most probable normalised mode shape matrix $\mathbf{U}$

Using the NLLF in Eq.(29), the MPV of the normalised mode shape matrix $\mathbf{U}$ is investigated in this section. Since the NLLF depends on $\mathbf{U}$ through the last two (quadratic) terms in the NLLF, the MPV of $\mathbf{U}$ must minimise the latter, which can be written as:

$$\begin{aligned} L_Q &= S_e^{-1}\left(d - d'\right) + \sum_k \mathcal{F}_k'^{*}\mathbf{E}_k'^{-1}\mathcal{F}_k' \\ &= S_e^{-1}d - S_e^{-1}\sum_k \mathcal{F}_k^{*}\mathbf{U}\left(\mathbf{I}_{n_g} - S_e\mathbf{E}_k'^{-1}\right)\mathbf{U}^T\mathcal{F}_k \end{aligned} \tag{33}$$

subjected to unit norm constraint of the partial mode shape in each synchronous group:

$$\left\|\overline{\mathbf{u}}_i\right\| = 1 \qquad\qquad i = 1,..., n_g \tag{34}$$

It is better to swap the order of $\mathcal{F}_k$ and $\mathbf{U}$ in Eq.(33) so that the MPV of $\mathbf{U}$ can be determined by solving eigenvalue problems. Rewrite $\mathbf{U}^T\mathcal{F}_k$ as

$$\mathbf{U}^T\mathcal{F}_k = \mathbf{F}_k\mathbf{U}' \tag{35}$$

where

$$\mathbf{F}_k = \begin{bmatrix} \mathcal{F}_{1k}^T & & \\ & \ddots & \\ & & \mathcal{F}_{n_g k}^T \end{bmatrix} \tag{36}$$

$$\mathbf{U}' = \begin{bmatrix} \overline{\mathbf{u}}_1 \\ \vdots \\ \overline{\mathbf{u}}_{n_g} \end{bmatrix} \tag{37}$$

Here, $\mathcal{F}_{ik}$ $(i = 1,...,n_g)$ is the FFT of the measured data corresponding to the ith synchronous data groups. The resulting L_Q can then be expressed as

$$L_Q = S_e^{-1}d - S_e^{-1}\mathbf{U}'^T\mathbf{A}\mathbf{U}' \tag{38}$$

where

$$\mathbf{A} = \sum_k \mathbf{F}_k^{*}\left(\mathbf{I}_{n_g} - S_e\mathbf{E}_k'^{-1}\right)\mathbf{F}_k \tag{39}$$

In order to apply the unit norm constraint in Eq.(34), it is better to express $\overline{\mathbf{u}}_i$ in terms of $\mathbf{U}'$ to facilitate analysis. Define a selection matrix $\mathbf{L}_i \in R^{n_i \times n}$ such that

$$\overline{\mathbf{u}}_i = \mathbf{L}_i \mathbf{U}' \tag{40}$$

where the (j,k)-entry of $\mathbf{L}_i$ is equal to 1 if DOF k is measured by the jth channel in the i th synchronous group, and zero otherwise. The Lagrangian for this constrained optimisation problem is then given by

$$J = S_e^{-1} d - S_e^{-1} \mathbf{U}'^T \mathbf{A} \mathbf{U}' + \sum_{i=1}^{n_g} q_i \left(\mathbf{U}'^T \mathbf{L}_i^T \mathbf{L}_i \mathbf{U}' - 1 \right) \tag{41}$$

where $\{q_i\}_{i=1}^{n_g}$ are the Lagrange multipliers that enforce the norm of $\overline{\mathbf{u}}_i \left(i = 1..., n_g \right)$ to be 1. The gradient of J with respect to $\mathbf{U}'$ is given by

$$\nabla_{\mathbf{U}'} J = -2 S_e^{-1} \mathbf{A} \mathbf{U}' + 2 \sum_{i=1}^{n_g} q_i \mathbf{L}_i^T \mathbf{L}_i \mathbf{U}' \tag{42}$$

The MPV of $\mathbf{U}'$ now can be obtained by solving $\nabla_{\mathbf{U}'} J = \mathbf{0}$, or equivalently

$$S_e^{-1} \mathbf{A} \mathbf{U}' = \sum_{i=1}^{n_g} q_i \mathbf{L}_i^T \mathbf{L}_i \mathbf{U}' \tag{43}$$

This is not a standard eigenvalue problem and evaluating the MPV of $\mathbf{U}'$ directly involves solving nonlinear equations. In view of this, the MPV of $\mathbf{U}'$ are updated in terms of $\overline{\mathbf{u}}_i$ in each synchronous group separately by assuming other $\overline{\mathbf{u}}_j$ ($i \neq j$) to be constant. Eq.(43) then can be written as:

$$\mathbf{A}_{ii} \overline{\mathbf{u}}_i + \sum_{j=1 (j \neq i)}^{n_g} \mathbf{A}_{ij} \overline{\mathbf{u}}_j = q_i \overline{\mathbf{u}}_i \qquad i = 1,..., n_g \tag{44}$$

where $\mathbf{A}_{ij} \in C^{n_i \times n_j}$ is the corresponding (i, j) partition matrix of $\mathbf{A}$. It now becomes a 'constrained eigenvalue problem' [36]. It can be shown that the MPV of $\overline{\mathbf{u}}_i$ can be obtained by taking the first half of the eigenvectors of $\mathbf{D}_i$ with largest eigenvalue and normalised to unit norm:

$$\mathbf{D}_i = \begin{bmatrix} \mathbf{A}_{ii} & \mathbf{b}_i \mathbf{b}_i^* \\ \mathbf{I}_{n_i} & \mathbf{A}_{ii} \end{bmatrix} \tag{45}$$

$$\mathbf{b}_i = \sum_{j=1(j\neq i)}^{n_g} \mathbf{A}_{ij} \bar{\mathbf{u}}_j \tag{46}$$

6. Most probable value of spectral parameters

The MPV of spectral parameters can be obtained through numerical optimisation of the NLLF in Eq.(29) with the constraints:

$$\sum_{i=1}^{n_g} \|\mathbf{u}_i\|^2 = 1 \tag{47}$$

due to the unit norm of the global mode shape and

$$\chi_{ij} \leq 1 \tag{48}$$

Without resorting to brute-force numerical techniques, it is more efficient to adopt a parameterisation that automatically takes care of these constraints. For the constraints in Eq.(47), the square norm of the partial mode shapes can be transferred to the scaling of the modal force PSD so that the resulting variable is unconstrained. Specifically, define

$$S_i = \sqrt{S}\,\|\mathbf{u}_i\| \qquad\qquad i = 1,...,n_g \tag{49}$$

which now become unconstrained variables. The condensed PSD matrix $\mathbf{E}'_k$ then can be expressed as:

$$\mathbf{E}'_k = D_k \, diag\{S_i\} \boldsymbol{\chi} \, diag\{S_i\} + S_e \mathbf{I}_{n_g} \tag{50}$$

In order to automatically satisfy the constraint in Eq.(48), χ_{ij} is parameterised through the angles $u_{ij}, v_{ij} \in R^n \left(i = 1,...,n_g; j < i\right)$ such that

$$\chi_{ij} = \left(\sin u_{ij}\right) \exp\left(\mathbf{i} v_{ij}\right) \tag{51}$$

Using the foregoing representations, the unconstrained parameters S_i and $\{u_{ij}, v_{ij}\}$ can be used for optimisation in place of S, $\{\|\mathbf{u}_i\|\}$ and $\{\chi_{ij}\}$. Once the MPV of S_i and $\{u_{ij}, v_{ij}\}$ have been found, the MPV of S, $\{\|\mathbf{u}_i\|\}$ and $\{\chi_{ij}\}$ can be recovered. Specifically

$$\hat{S} = \sum_{i=1}^{n_g} \hat{S}_i^2 \tag{52}$$

$$\left\| \hat{\mathbf{u}}_i \right\| = \frac{\hat{S}_i^2}{\sqrt{\sum_{i=1}^{n_g} \hat{S}_i^2}} \qquad i = 1,..., n_g \tag{53}$$

where a hat '^' denotes MPV.

7. High signal-to-noise asymptotics

In this section, the asymptotic behaviour of some parameters is investigated under high signal-to-noise (s/n ratio) condition, i.e., the modal signal is much larger than the prediction error, which is often met in well-controlled field tests. It turns out that the asymptotic MPVs of $\{\overline{\mathbf{u}}_i\}$, S_e and S_i can be obtained directly based on the measured data, which can also provide good initial guesses for the iterative procedure to be proposed in the next section.

7.1 Asymptotic MPV of $\{\overline{\mathbf{u}}_i\}$

The high s/n ratio condition for $\mathbf{A}$ in Eq.(39) here refers to the case when

$$\mathbf{I}_{n_g} - S_e \mathbf{E}_k'^{-1} \sim \mathbf{I}_{n_g} \tag{54}$$

In this case

$$\mathbf{A} \sim \sum_k \mathbf{F}_k^* \mathbf{F}_k \tag{55}$$

which becomes a constant matrix with off-diagonal partitions equal to zero. This implies that there is no cross term between $\overline{\mathbf{u}}_i$ and $\overline{\mathbf{u}}_j$ for $i \neq j$ in Eq.(44), which can be expressed as:

$$\mathbf{A}_{ii} \overline{\mathbf{u}}_i = \lambda_i \overline{\mathbf{u}}_i \qquad i = 1,..., n_g \tag{56}$$

The asymptotic MPV of $\overline{\mathbf{u}}_i$ now can be obtained by solving a standard eigenvalue problem. It follows that the eigenvector of $\mathbf{A}_{ii}$ with the largest eigenvalue is the MPV of $\overline{\mathbf{u}}_i$ (normalised to unit norm).

7.2 Asymptotic MPV of prediction error

For high s/n ratio condition, $\mathbf{E}_k'$ in Eq.(24) is dominated by the modal response (i.e., the first term) and hence asymptotically independent of the prediction error S_e. In this context, the

NLLF only depends on S_e through the first and third term in Eq.(29). Rewrite these two terms as:

$$\left(n-n_g\right)N_f \ln S_e + S_e^{-1}\left(d-d'\right) = \left(n-n_g\right)N_f \left\{\ln S_e + S_e^{-1}\left[\left(d-d'\right)/\left(n-n_g\right)N_f\right]\right\} \tag{57}$$

which are of the form $\ln x + c/x$. This form has a unique minimum of $1+\ln c$ at $x=c$. The high s/n asymptotic MPV of S_e can now be obtained as:

$$\hat{S}_e \sim \left(d-d'\right)/\left(n-n_g\right)N_f \tag{58}$$

7.3 Asymptotic MPV of S_i

The asymptotic MPV of S_i cannot be directly obtained from the NLLF in Eq.(29) under high s/n ratio condition as the determinant of $\mathbf{E}_k'$ depends non-trivially on $\boldsymbol{\chi}$ (see Eq.(50)). In this context, its analytical form still cannot be explicitly expressed in terms of S_i. However, the asymptotic MPV of S_i can be estimated by making use of the fact that the data in different groups share the same modal force PSD. When analysing the data of different groups separately, the identified value of modal force PSD in each group is scaled by the squared norm of the partial mode shape measured by this group (as the partial mode shape is normalised to have unit norm). Since the data channels in each group are synchronised, its asymptotic value can be obtained based on an existing fast Bayesian formula that assumes synchronous data [37]. Specifically,

$$\hat{S}_i \sim \sqrt{N_f^{-1}\sum_{k=1}^{N_f} \overline{\mathbf{u}}_i^T D_k^{-1} \mathcal{F}_{ik} \mathcal{F}_{ik}^* \overline{\mathbf{u}}_i} \tag{59}$$

for $i = 1,...,n_g$.

8. Summary of procedure

Based on the foregoing analysis, an iterative procedure for determining the MPV of modal parameters is summarised in this section. Instead of optimising all the parameters simultaneously, the proposed method optimises them in groups (given the remaining parameters) and iterates until convergence. Different groups have been investigated (details omitted here) and it is found that optimising $\{u_{ij}, v_{ij}\}$, $\{f, \zeta\}$, $\{S_i\}$, S_e, $\{\overline{\mathbf{u}}_i\}$ sequentially and

iteratively leads to a good modal identification algorithm balancing robustness and efficiency. The optimisation scheme is summarised as follows:

Step I. Initial Guess

1) Calculate the FFT of measured data.
2) Select the frequency band for the mode of interest.
3) Pick the initial guess of f from the singular value spectrum and set the initial guess of ζ as 1% (say).
4) Take the initial guess of $\overline{\mathbf{u}}_i \ \left(i = 1,...,n_g\right)$ as the eigenvector with the largest eigenvalue of $\mathbf{A}_{ii}$ in Eq.(56).
5) Calculate the initial guess of S_e using Eq.(58).
6) Calculate the initial guess of $S_i \ \left(i = 1,...,n_g\right)$ using Eq.(59).
7) The angles $\left\{u_{ij}, v_{ij}\right\}$ can be nominally assigned as 0.1.

Step II. Iteration Phase

In the following, parameters that are not updated are kept at their current value during iteration.

1) Update $\left\{u_{ij}, v_{ij}\right\}$ by minimising L in Eq.(29) with respect to $\left\{u_{ij}, v_{ij}\right\}$.
2) Update $\left\{f, \zeta\right\}$ by minimising L in Eq.(29) with respect to $\left\{f, \zeta\right\}$.
3) Update $\left\{S_i\right\}$ by minimising L in Eq.(29) with respect to $\left\{S_i\right\}$.
4) Update S_e by minimising L in Eq.(29) with respect to S_e.
5) Update $\overline{\mathbf{u}}_i \ \left(i = 1,...,n_g\right)$ as the first half of the eigenvectors of $\mathbf{D}_i$ in Eq.(45) with the largest eigenvalue and normalised to unit norm.

Repeat Steps 1) to 5) until convergence.

Step III. MPV of S and $\boldsymbol{\varphi}$

1) Obtain the MPV of S using Eq.(52).
2) Obtain the MPV of $\left\{\left\|\mathbf{u}_i\right\|\right\}$ using Eq.(53).
3) Obtain the MPV of global mode shape $\boldsymbol{\varphi}$ by

$$\hat{\boldsymbol{\varphi}} = \begin{bmatrix} s_1 \left\| \hat{\mathbf{u}}_1 \right\| \hat{\bar{\mathbf{u}}}_1 \\ \vdots \\ s_i \left\| \hat{\mathbf{u}}_i \right\| \hat{\bar{\mathbf{u}}}_i \\ \vdots \\ s_{n_g} \left\| \hat{\mathbf{u}}_{n_g} \right\| \hat{\bar{\mathbf{u}}}_{n_g} \end{bmatrix} \tag{60}$$

where $s_i = \pm 1 \left(i = 1,...,n_g \right)$ is the sign of the relative direction between partial mode shapes. It should be noted that swapping the sign of the coherence value and the partial mode shapes gives the same $\mathbf{E}_k$ and hence the NLLF. Without additional assumptions on the sign of coherence (e.g., the coherence value may be positive in the low frequency range when the synchronisation degree between two synchronous data groups are high), the relative direction between partial mode shapes cannot be directly identified. This is one fundamental limitation when dealing with asynchronous ambient data. In real implementation, the relative direction among partial mode shapes can be either determined intuitively based on spatial continuity or an empirical analysis of the coherence among different groups.

9. Illustrative examples

Three examples are presented in this section to illustrate the proposed method and its practical application. The first example is based on synthetic data, which serves to verify consistency of the algorithm. The proposed method is applied to modal identification of laboratory data in the second example, which investigates the applicability to real asynchronous data under well controlled environment. In the third example, a full-scale ambient vibration test based on asynchronous data is presented. It illustrates the feasibility of the proposed method to asynchronous ambient data measured under field test conditions, where complications and practical issues are naturally reflected in the data. The identification results based on the proposed method are also compared with the ones identified based on synchronous data and asynchronous data using the previously developed Bayesian method that assumes zero coherence among synchronous data groups in the laboratory and field test examples.

9.1 Synthetic example

Consider a six-storey shear building with a uniform inter-storey stiffness of 2000kN/mm and floor mass of 500 tons. The resulting natural frequencies of the first four modes are 2.427Hz, 7.139Hz, 11.436Hz and 15.069Hz, respectively. The damping ratios of these modes are

assumed to be 1%. The structure is subjected to i.i.d. Gaussian white noise excitation with a PSD of $9.81\text{N}/\sqrt{\text{Hz}}$ in the lateral direction of each floor, which is typical in ambient vibration tests. Assume two synchronous data groups in this test, measuring the vibration responses of 1/F to 3/F and 4/F to 6/F, respectively. Figure 1 shows the schematic diagram of this example. To simulate the asynchronous data, the coherences of the modal excitations among these two groups are taken to be 0.8, 0.6, 0.6, 0.5 for the first four modes, respectively. The measurement noise is taken to be i.i.d. Gaussian white noise with a (root) PSD of $3\mu\text{g}\sqrt{\text{Hz}}$ for all data channels, which is the typical noise level of force-balanced accelerometers. The acceleration response for 20 minutes with a sampling rate of 100Hz is assumed to be available for modal analysis.

Figure 2 shows the root singular value spectrum of the data. Modal identification of the first four modes was conducted using the proposed method. The selected initial guesses of natural frequencies and the associated frequency bands for modal identification are shown with symbols ‘o’ and ‘[-]’ in the figure, respectively. An additional peak can be found in each frequency band of the mode of interest, which is due to the asynchronous nature of the data. Table 1 summaries the MPV of modal parameters as well as their exact values that generated the data. It can be seen that the identified modal parameters are very close to their exact values, verifying the consistency of the proposed method. The MPV of prediction error PSD tends to be larger than the assumed values for higher modes, which is mainly due to modelling error from the contribution of the non-resonant part of lower modes. The mode shape MPVs and exact values agree well with each other with MAC (modal assurance criterion) values between these two extremely close to 1 (up to 4 decimal points). The identified coherence values for Mode 1, Mode 2 and Mode 4 agree well with the exact ones. Small discrepancies can be found in the phase of coherence MPV for Mode 3. This can be due to the contribution of Mode 2 and Mode 4 (since there are not well apart from Mode 3) as well as the measurement noise.

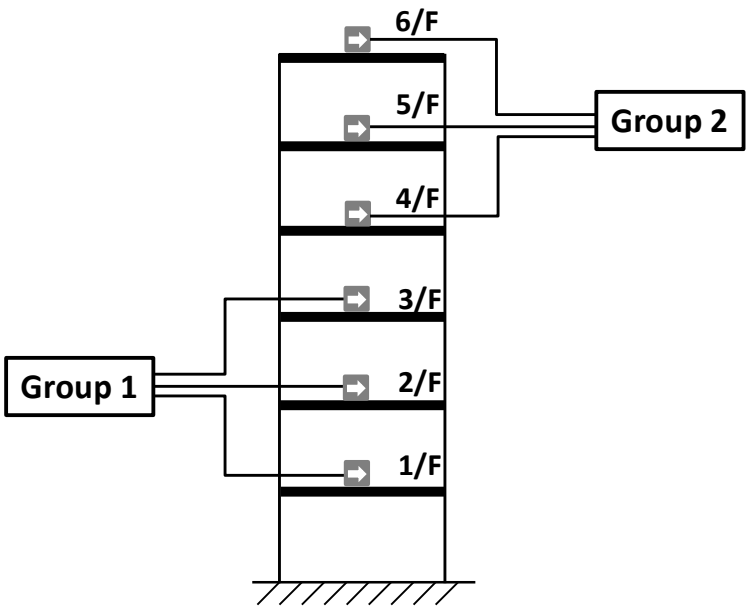

Figure 1. Schematic Diagram, Synthetic Data Example

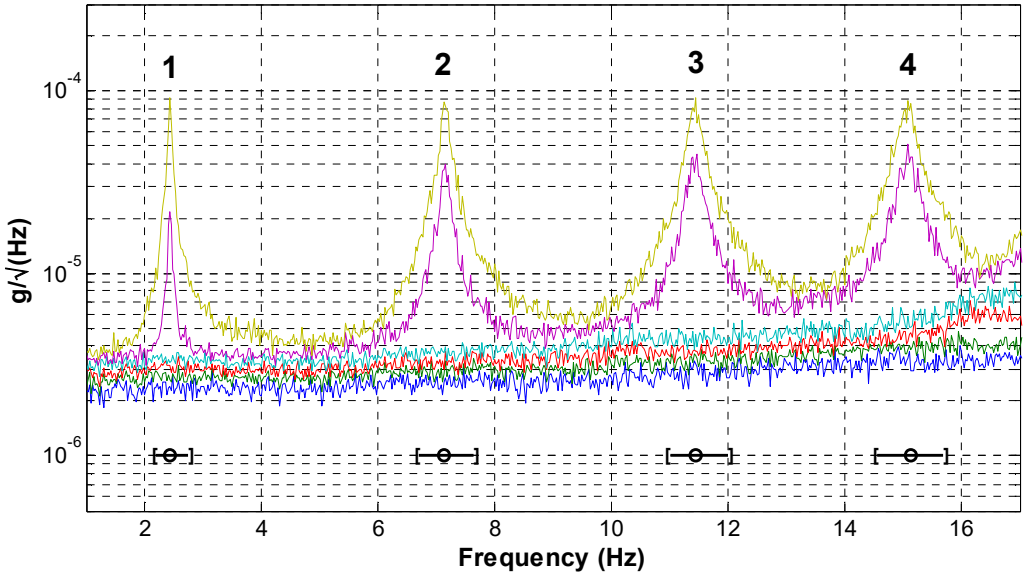

Figure 2. Root Singular Value Spectrum, Synthetic Data Example

Table 1. Identified Modal Parameters (MPV), Synthetic Data Example

Mode	f (Hz)		ζ (%)		$\sqrt{S}$ (μg/√Hz)		$\sqrt{S_e}$ (μg/√Hz)		χ	
	MPV	Exact	MPV	Exact	MPV	Exact	MPV	Exact	MPV	Exact
1	2.427	2.427	0.99	1.00	2.00	2.00	2.98	3.00	0.81	0.80
2	7.143	7.139	1.07	1.00	2.03	2.00	3.19	3.00	0.61	0.60
3	11.432	11.436	1.04	1.00	1.95	2.00	3.67	3.00	0.56-0.24**i**	0.60

4	15.071	15.069	1.01	1.00	1.88	2.00	4.49	3.00	0.50	0.50

9.2 Laboratory example

A four-storey laboratory shear frame (shown in Figure 3) is considered, measuring $30\text{cm} \times 20\text{cm}$ in plan with a uniform storey height of 25cm. It is considered before in Section 9.2 of [33]. Six piezoelectric accelerometers distributed at the centre of each storey are used to measure the vibration response of the structure in the horizontal direction (i.e., one data channel for each sensor). Channel 1 to 4 are synchronised using one DAQ unit and Channel 5 & 6 are synchronised using another. These two DAQ units are controlled to start and finish measuring at the same time but use their own clocks for data sampling.

Thirty minutes of ambient vibration response were measured with a sampling rate of 2048Hz (later decimated to 256Hz for analysis) for all data channels. The data measured by channel 1 to 4 are combined and referred to as the synchronous data set while the data measured by channel 1,2,5,6 are combined and referred to as the asynchronous data set. Modal identification for the synchronous data set has been conducted using the fast Bayesian FFT method for synchronous data [37] and that for the asynchronous data set has been conducted using the proposed method. The identification results based on the synchronous data set are used as the reference values in this example.

Figure 4 shows the root singular value spectrum of the asynchronous data set. The first five modes shown in the spectrum are selected for modal analysis. Similar to the synthetic data example, the initial guesses of natural frequencies and selected bands are shown in the figure with symbols ‘o’ and ‘[-]’, respectively. The identified modal parameters from the synchronous data, the asynchronous data using method based on zero coherence assumption [33] and the proposed method are listed Table 2. It can be seen that the MPVs of modal parameters determined by the proposed method based on the asynchronous data set almost coincide with the synchronous counterparts. The identification results illustrate that the proposed method provides a good estimation of the modal parameters based on real asynchronous data. The method with zero coherence assumption [33] could also provide a precise estimation of modal parameters. The proposed method is capable of quantifying the coherence values among synchronous data groups but does not have a significant improvement in the identification accuracy of modal parameters compared to the method with zero coherence assumption.

Figure 3. Four-storey Shear Frame

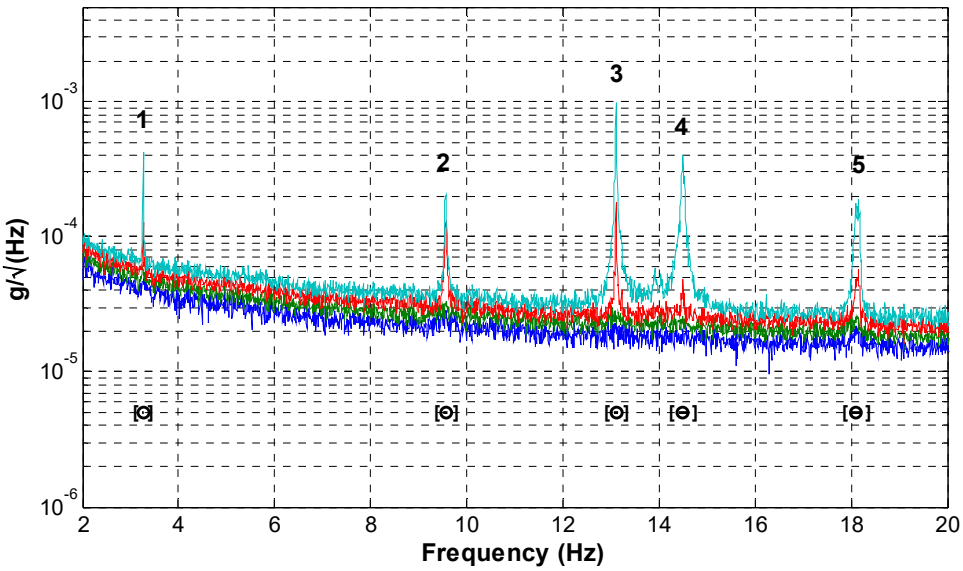

Figure 4. Root Singular Value Spectrum of Asynchronous Data Set, Laboratory Example

Table 2. Identified Modal Parameters (MPV), Laboratory Example

Modal parameters		Mode				
		1	2	3	4	5
f(Hz)	Syn.	3.260	9.559	13.108	14.496	18.128
	Asyn. (Zero Coh.)	3.260	9.560	13.108	14.496	18.128
	Asyn. (Gen. Coh.)	3.260	9.560	13.108	14.496	18.128
ζ(%)	Syn.	0.07	0.15	0.04	0.15	0.22

$\sqrt{S}\left(\mu g/\sqrt{Hz}\right)$	Asyn. (Zero Coh.)	0.08	0.15	0.04	0.15	0.23
	Asyn. (Gen. Coh.)	0.08	0.14	0.04	0.15	0.22
	Syn.	0.89	0.76	1.03	1.21	0.83
	Asyn. (Zero Coh.)	0.97	0.74	1.05	1.21	0.83
	Asyn. (Gen. Coh.)	0.97	0.73	1.05	1.21	0.82
$\sqrt{S_e}\left(\mu g/\sqrt{Hz}\right)$	Syn.	54.1	28.1	25.1	23.5	22.0
	Asyn. (Zero Coh.)	54.1	28.9	22.9	20.5	22.7
		50.1	27.8	23.8	22.9	21.1
	Asyn. (Gen. Coh.)	52.3	28.3	23.4	21.8	22.0
$\boldsymbol{\varphi}$(MAC)	Syn.	N/A	N/A	N/A	N/A	N/A
	Asyn. (Zero Coh.)	0.9995	0.9998	0.9975	0.9998	0.9999
	Asyn. (Gen. Coh.)	0.9998	0.9999	0.9974	0.9999	0.9999
χ	Asyn. (Gen. Coh.)	0.77-0.63i	0.37+0.93i	0.90+0.45i	0.98+0.17i	0.85-0.52i

9.3 Field test example

The instrumented structure in this example is Brodie Tower at the University of Liverpool, which was previously considered in Section 4.4 of [34] for the illustration of the Bayesian OMA method with zero coherence assumption. It is an eight-storey reinforced-concrete building with a height of approximately 25m. The ground floor of the building is connected to another office building with a shape close to a rectangle, see Figure 5. The remaining floors are T-shaped measuring $25\text{m}\times 28\text{m}$ in plan.

Four force-balanced accelerometers were deployed to measure the ambient vibration response of the structure on the sixth floor. The test focused on the lateral modes of the building, where biaxial acceleration data at four locations are used for analysis. Figure 5 shows the plan view of the building with measurement locations marked as squares. Asynchronous data were first measured where each accelerometer used its own clock for sampling. After obtaining the asynchronous data, the sensors were synchronised using GPS and the synchronous data were measured. Twenty minutes of ambient data were collected with a sampling rate of 50Hz for both asynchronous and synchronous data. Within the frequency range of interest, the overall channel noise is in the order of $0.5\mu g/\sqrt{Hz}$.

The root singular value spectrum of the measured asynchronous data is shown in Figure 6. Modal identification focuses on the first six modes marked in the figure. The initial guesses of natural frequency (hand-picked) and selected frequency bands are also indicated in the figure. Modal identification for asynchronous data has been conducted using the Bayesian method that assumes zero coherence [33] and the proposed method with general coherence

assumption, respectively. The modal parameters for synchronous data are identified using the Bayesian FFT method that assumes synchronous data [37]. Identification results are summarised in Table 3. For asynchronous data, the identified modal parameters based on the proposed method almost coincide with those based on the Bayesian method with zero coherence assumption. They are also close to the synchronous counterparts. Small discrepancies can be found. These are mainly due to environmental variations as asynchronous and synchronous data were measured at different time periods.

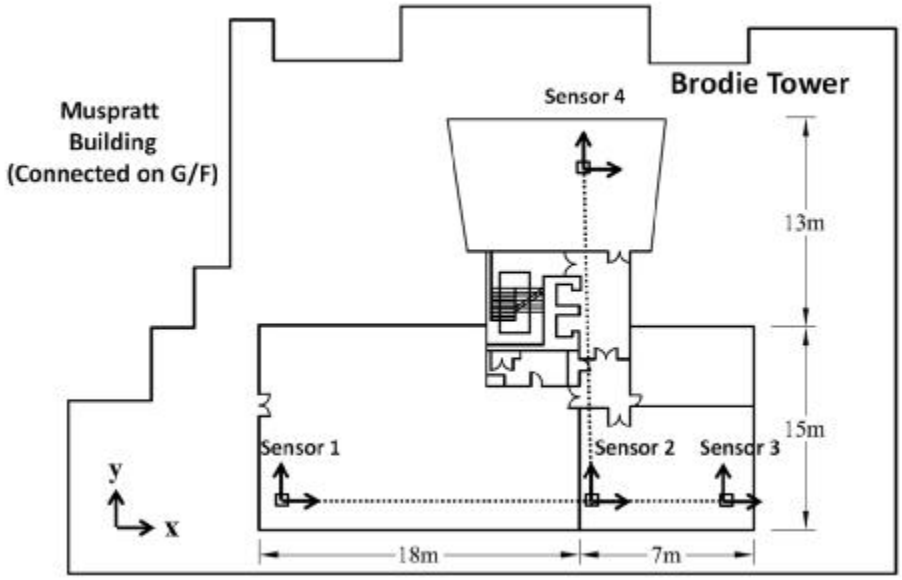

Figure 5. Plan View with Measurement Locations

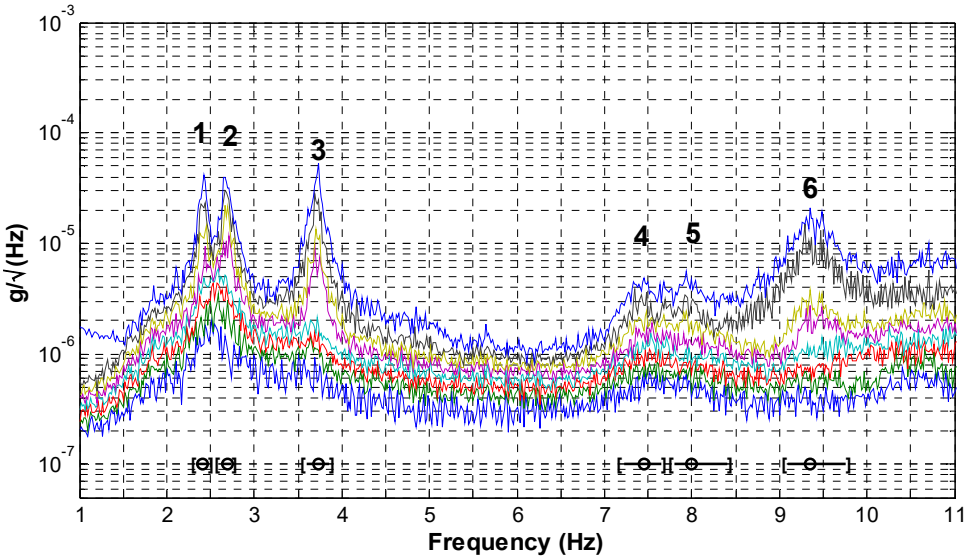

Figure 6. Root Singular Value Spectrum of Asynchronous Data Set, Field Test Example

Table 3. Identified Modal Parameters (MPV), Field Test Example

Modal parameters		Mode					
		1	2	3	4	5	6
f (Hz)	Syn.	2.428	2.698	3.751	7.379	7.983	9.441
	Asyn. (Zero Coh.)	2.418	2.678	3.714	7.419	7.932	9.391
	Asyn. (Gen. Coh.)	2.417	2.679	3.714	7.420	7.932	9.390
$\zeta(\%)$	Syn.	1.14	0.94	0.78	2.43	3.20	2.33
	Asyn. (Zero Coh.)	1.32	1.08	0.90	2.21	2.41	1.97
	Asyn. (Gen. Coh.)	1.18	1.16	0.89	2.20	2.16	1.95
$\sqrt{S}\left(\mu g/\sqrt{Hz}\right)$	Syn.	1.10	1.01	0.80	0.22	0.32	0.80
	Asyn. (Zero Coh.)	1.28	1.32	1.05	0.24	0.27	0.77
	Asyn. (Gen. Coh.)	1.20	1.37	1.05	0.24	0.25	0.77
$\sqrt{S_e}\left(\mu g/\sqrt{Hz}\right)$	Syn.	1.94	2.28	1.07	0.96	0.88	1.01
	Asyn. (Zero Coh.)	3.04	3.27	1.49	1.10	1.07	0.96
	Asyn. (Gen. Coh.)	3.04	3.27	1.49	1.10	1.09	0.96

Figure 7 to Figure 9 show the identified mode shapes (MPV) based on synchronous data, asynchronous data using Bayesian method with zero coherence assumption and the proposed method, respectively. The dashed line and the solid line denote the undeformed and deformed modes shapes, respectively. The squares represent the measurement locations (corresponding to the ones shown in Figure 5). Using the mode shape MPVs based on the synchronous data set as reference values, Table 4 shows the MAC values of the ones identified based on the proposed method and the zero coherence method, respectively. It can be seen that the identified mode shapes using the proposed method based on asynchronous data agree well with those based on the synchronous data. They are also close to those identified using the Bayesian method that assumes zero coherence. It can be seen that the MAC values based on these two methods are extremely close to 1, suggesting good quality in the identified mode shapes for both methods.

Table 5 shows the computational time for determining the MPVs of modal parameters in this example. It can be seen that modal identification based on asynchronous data takes more time than synchronous data. This is especially so for the proposed method. This is reasonable as compared to the other two methods, the dimension of matrix involved in the proposed method equals to the number of synchronous data groups (which is four in this example).

The foregoing results show that the proposed method can provide a good estimation quality of modal parameters based on asynchronous data. Compared to the previously developed Bayesian method that assumes zero coherence, the proposed method does not have a

significant improvement in the precision of modal parameter MPVs. It also takes longer time for the optimisation procedure. Nevertheless, the proposed method provides a feasible means for determining the MPVs of modal parameters where the asynchronous model is strictly obeyed. It can also investigate the time synchronisation degrees among different synchronisation data groups quantitatively by identifying the coherence values among the groups. Computations can be done in the order of minutes for the proposed method, which is still acceptable even for on site implementation.

Table 4. Mode Shape MAC values, Field Test Example

		Mode					
		1	2	3	4	5	6
MAC Values	Asyn. (Zero Coh.)	0.9994	0.9995	0.9994	0.9373	0.9794	0.9988
	Asyn. (Gen. Coh.)	0.9994	0.9995	0.9993	0.9345	0.9817	0.9988

Table 5. Computaional Time, Field Test Example

		Mode					
		1	2	3	4	5	6
Computational Time (s)	Syn.	1.2	1.0	0.9	3.5	4.1	2.8
	Asyn. (Zero Coh.)	3.4	3.2	3.4	26.6	31.8	27.7
	Asyn. (Gen. Coh.)	384.8	303.1	181.2	445.9	377.9	468.9

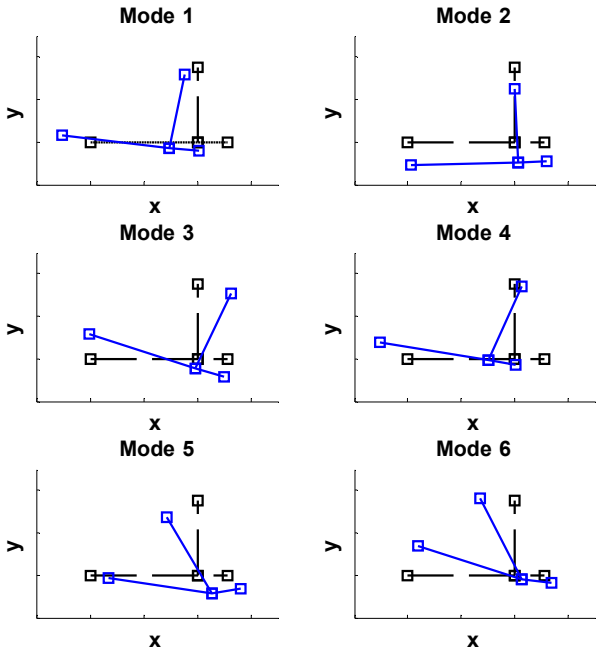

Figure 7. Mode Shape MPVs, Brodie Tower Synchronous Data

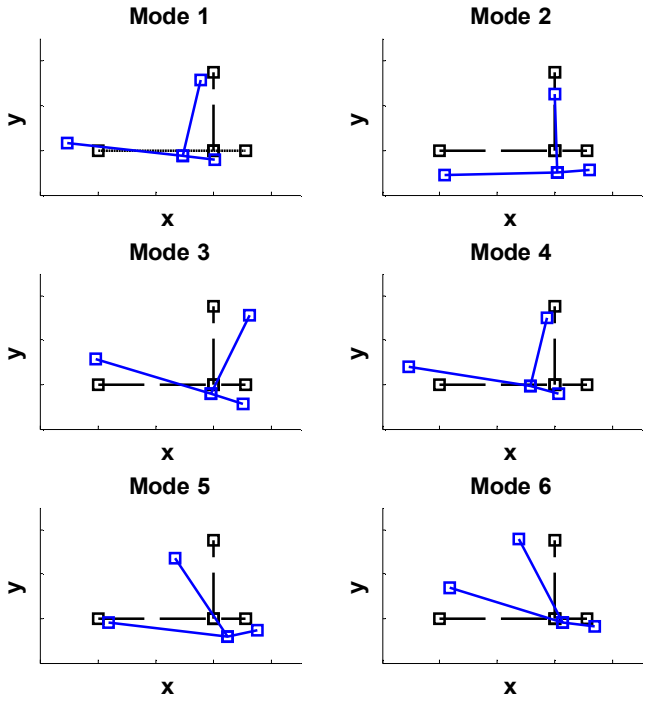

Figure 8. Mode Shape MPVs, Brodie Tower Asynchronous Data (Zero Coh.)

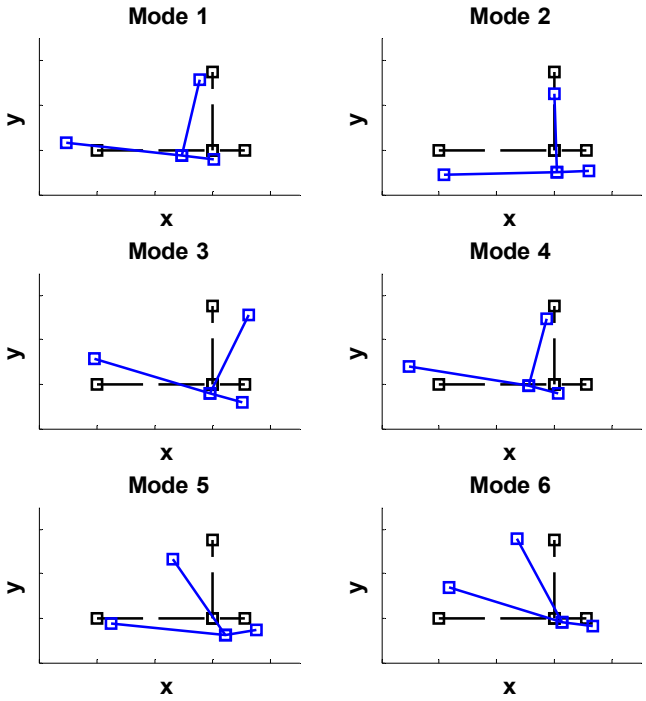

Figure 9. Mode Shape MPVs, Brodie Tower Asynchronous Data (Gen. Coh.)

10. Conclusions

A Bayesian frequency domain modal identification method for asynchronous ambient vibration data has been proposed in this work. It is developed based on an asynchronous data model that assumes imperfect coherence among different synchronisation data groups. Computational difficulties have been addressed and efficient strategies have been developed to determine the most probable value of model parameters as well as the coherence values. The NLLF is written in a condensed form where the matrix involved in computation has full rank with dimension equal to the number of synchronisation groups. The computational effort is thus significantly suppressed compared to that of the original formulation. The consistency of the proposed method has been demonstrated by the synthetic and laboratory data examples. An application with field data has also been presented. The study reveals that the proposed method provides a good identification quality of modal parameters using asynchronous ambient data.

Compared to the previously developed Bayesian OMA method with zero coherence assumption, the proposed method in this paper provides a feasible means to identify the modal parameters as well as coherence values from asynchronous data where the asynchronous model is strictly obeyed without extra modelling error involved. It should be noted that the proposed method does not lead to a significant improvement in the identification accuracy of modal parameters compared to the method with zero coherence assumption since the latter can already provide a good identification quality. In practice, the method with zero coherence assumption is preferred to avoid additional computational cost if one is not interested in quantifying the synchronisation degrees among different data groups.

This work mainly focuses on determining the MPV of modal parameters as well as the coherence values. The associated identification uncertainty shall be investigated in future work. It should be noted that although a condensed PSD matrix has been proposed in this paper to facilitate computation, the determinant and inverse of the theoretical PSD matrix are still not analytically tractable, which may lead to difficulties in deriving the posterior covariance matrix for uncertainty quantification. Asynchronisation in OMA is currently a challenging issue and it is hoped that this work provides some understanding on this problem and inspirations for further development of modal identification methods based on asynchronous ambient data.

Acknowledgement

This paper is partially supported by UK Engineering & Physical Research Council (EP/N017897/1). The financial support is gratefully acknowledged.

References

[1] R. Brincker, C.E. Ventura, Introduction to Operational Modal Analysis, Wiley, London, 2015. doi:10.1002/9781118535141.

[2] S.-K. Au, Operational Modal Analysis: Modeling, Bayesian Inference, Uncertainty Laws, Springer, 2017.

[3] S. Beskhyroun, L.D. Wegner, B.F. Sparling, New methodology for the application of vibration-based damage detection techniques, Struct. Control Heal. Monit. (2011). doi:10.1002/stc.

[4] G. Hearn, R. Testa, Modal analysis for damage detection in structures, J. Struct. Eng. 117 (1991) 3042–3063.

[5] C.R. Farrar, K. Worden, An introduction to structural health monitoring., Philos. Trans. A. Math. Phys. Eng. Sci. 365 (2007) 303–315. doi:10.1098/rsta.2006.1928.

[6] F.N. Catbas, T. Kijewski-Correa, A.E. Aktan, Structural identification (St-Id) of constructed facilities: Approaches, methods and technologies for effective practice of St-Id, in: Am Soc Civ Eng, 2011.

[7] S.S. Ivanović, M.D. Trifunac, E.I. Novikova, a. a. Gladkov, M.I. Todorovska, Ambient vibration tests of a seven-story reinforced concrete building in Van Nuys, California, damaged by the 1994 northridge earthquake, Soil Dyn. Earthq. Eng. 19 (2000) 391–411. doi:10.1016/S0267-7261(00)00025-7.

[8] H. Wenzel, D. Pichler, Ambient vibration monitoring, Wiley, UK, 2005.

[9] J.M.W. Brownjohn, Structural health monitoring of civil infrastructure., Philos. Trans. A. Math. Phys. Eng. Sci. 365 (2007) 589–622. doi:10.1098/rsta.2006.1925.

[10] J.S. Bendat, A.G. Piersol, Engineering applications of correlation and spectral analysis., New York: Wiley, 1980., 1980.

[11] R. Brincker, L. Zhang, P. Andersen, Modal identification of output-only systems using frequency domain decomposition, Smart Mater. Struct. 10 (2001) 441–445. doi:10.1088/0964-1726/10/3/303.

[12] I. James, George H., T.G. Carne, J.P. Lauffer, The natural excitation technique (NExT) for modal parameter extraction from operating structures, Int. J. Anal. Exp. Modal Anal. 10 (1995) 260–277.

[13] B. Peeters, G. De Roeck, Reference-Based Stochastic Subspace Identification for Output-Only Modal Analysis, Mech. Syst. Signal Process. 13 (1999) 855–878. doi:10.1006/mssp.1999.1249.

[14] P. Van Overschee, B.L. De Moor, Subspace identification for linear systems: Theory—Implementation—Applications, Springer Science & Business Media, 2012.

[15] K.V. Yuen, L.S. Katafygiotis, Bayesian time-domain approach for modal updating using ambient data, Probabilistic Eng. Mech. 16 (2001).

[16] L.S. Katafygiotis, K.V. Yuen, Bayesian spectral density approach for modal updating using ambient data, Earthq. Eng. Struct. Dyn. 30 (2001) 1103–1123. doi:10.1002/eqe.53.

[17] W.-J. Yan, L.S. Katafygiotis, A two-stage fast Bayesian spectral density approach for ambient modal analysis. Part I: Posterior most probable value and uncertainty, Mech. Syst. Signal Process. 54 (2015) 139–155. doi:10.1016/j.ymssp.2014.07.027.

[18] W.-J. Yan, L.S. Katafygiotis, A two-stage fast Bayesian spectral density approach for ambient modal analysis. Part II: Mode shape assembly and case studies, Mech. Syst. Signal Process. 54 (2015) 156–171. doi:10.1016/j.ymssp.2014.08.016.

[19] K.V. Yuen, L.S. Katafygiotis, Bayesian fast Fourier transform approach for modal updating using ambient data, Adv. Struct. Eng. 6 (2003) 81–95.

[20] S.-K. Au, F.-L. Zhang, Y.-C. Ni, Bayesian operational modal analysis: Theory, computation, practice, Comput. Struct. 126 (2013) 3–14. doi:10.1016/j.compstruc.2012.12.015.

[21] F.L. Zhang, H.B. Xiong, W.X. Shi, X. Ou, Structural health monitoring of Shanghai Tower during different stages using a Bayesian approach, Struct. Control Heal. Monit.

23 (2016) 1366–1384.

[22] J. Hu, H. Lam, J. Yang, Operational modal identification and finite element model updating of a coupled building following Bayesian approach, Struct. Control Heal. Monit. 25 (2018) e2089.

[23] S.-C. Kuok, K.-V. Yuen, Investigation of modal identification and modal identifiability of a cable-stayed bridge with Bayesian framework, Smart Struct. Syst. 17 (2016) 445–470.

[24] S.-C. Kuok, K.-V. Yuen, Structural health monitoring of Canton Tower using Bayesian framework, Smart Struct. Syst. 10 (2012) 375–391.

[25] D.L. Mills, Internet time synchronization: the network time protocol, IEEE Trans. Commun. 39 (1991) 1482–1493. doi:10.1109/26.103043.

[26] E. Kaplan, C. Hegarty, Understanding GPS: principles and applications, Artech house, 2005.

[27] J.P. Lynch, A Summary Review of Wireless Sensors and Sensor Networks for Structural Health Monitoring, Shock Vib. Dig. 38 (2006) 91–128. doi:10.1177/0583102406061499.

[28] Y. Lei, A.S. Kiremidjian, K.K. Nair, J.P. Lynch, K.H. Law, Algorithms for time synchronization of wireless structural monitoring sensors, Earthq. Eng. Struct. Dyn. 34 (2005) 555–573. doi:10.1002/eqe.432.

[29] J. Elson, L. Girod, D. Estrin, Fine-grained network time synchronization using reference broadcasts, ACM SIGOPS Oper. Syst. Rev. 36 (2002) 147–163. doi:10.1145/844128.844143.

[30] S. Bjorklund, L. Ljung, A review of time-delay estimation techniques, in: 42nd IEEE Int. Conf. Decis. Control (IEEE Cat. No.03CH37475), 2003: pp. 2502–2507. doi:10.1109/CDC.2003.1272997.

[31] G. Jacovitti, G. Scarano, Discrete time techniques for time delay estimation, IEEE Trans. Signal Process. 41 (1993) 525–533. doi:10.1109/78.193195.

[32] Y.-C. Zhu, S.-K. Au, Spectral characteristics of asynchronous data in operational

modal analysis, Struct. Control Heal. Monit. (2017) e1981. doi:10.1002/stc.1981.

[33] Y.-C. Zhu, S.-K. Au, Bayesian Operational Modal Analysis with Asynchronous Data, Part I: Most Probable Value., Mech. Syst. Signal Process. 98C (2018) 652–666.

[34] Y.-C. Zhu, S.-K. Au, Bayesian Operational Modal Analysis with Asynchronous Data, Part II: Posterior Uncertainty., Mech. Syst. Signal Process. 98C (2018) 920–935.

[35] D.R. Brillinger, Time series: data analysis and theory, Siam, 1981.

[36] W. Gander, G.H. Golub, U. von Matt, A constrained eigenvalue problem, Linear Algebra Appl. 114–115 (1989) 815–839. doi:10.1016/0024-3795(89)90494-1.

[37] S.-K. Au, Fast Bayesian FFT method for ambient modal identification with separated modes, J. Eng. Mech. (2011). doi:10.1061/(ASCE)EM.1943-7889.0000213.